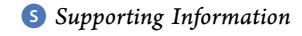


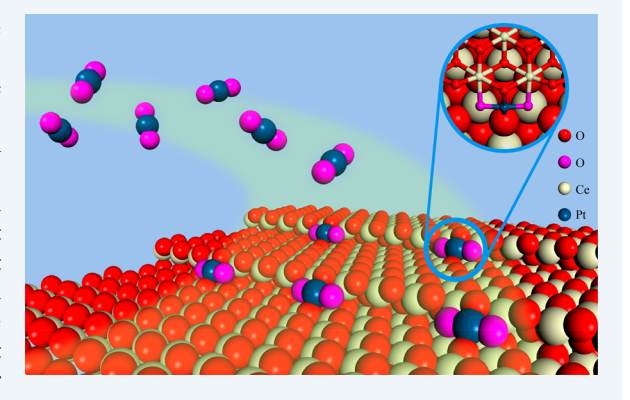
Stabilizing High Metal Loadings of Thermally Stable Platinum Single **Atoms on an Industrial Catalyst Support**

Deepak Kunwar,[†] Shulan Zhou,^{‡,§} Andrew DeLaRiva,[†] Eric J. Peterson,[†] Haifeng Xiong,[†] Xavier Isidro Pereira-Hernández,^{||} Stephen C. Purdy,[†] Rik ter Veen,[#] Hidde H. Brongersma,^{#,7} Jeffrey T. Miller,[†] Hiroki Hashiguchi,⁸ Libor Kovarik,⁹ Sen Lin,^{*,10} Hua Guo,[‡] Yong Wang,^{*,||,9} and Abhaya K. Datye*, Too

¹⁰State Key Laboratory of Photocatalysis on Energy and Environment, College of Chemistry, Fuzhou University, Fuzhou 350002,



ABSTRACT: Single-atom catalysts have attracted attention because of improved atom efficiency, higher reactivity, and better selectivity. A major challenge is to achieve high surface concentrations while preventing these atoms from agglomeration at elevated temperatures. Here we investigate the formation of Pt single atoms on an industrial catalyst support. Using a combination of surface sensitive techniques such as XPS and LEIS, X-ray absorption spectroscopy, electron microscopy, as well as density functional theory, we demonstrate that cerium oxide can support Pt single atoms at high metal loading (3 wt % Pt), without forming any clusters or 3D aggregates when heated in air at 800 °C. The mechanism of trapping involves a reaction of the mobile PtO2 with under-coordinated cerium cations present at CeO₂(111) step edges, allowing Pt to achieve a stable square planar configuration. The strong interaction of mobile single-atom species



with the support, present during catalyst sintering and regeneration, helps explain the sinter resistance of ceria-supported metal catalysts.

KEYWORDS: single-atom catalysis, thermal stability, ionic Pt, catalyst preparation, atom trapping

1. INTRODUCTION

Single-atom catalysts¹ represent a new frontier in heterogeneous catalysis because of improved atom efficiency, higher reactivity, and improved selectivity for a range of catalytic reactions.²⁻⁵ However, isolated atoms become mobile at elevated temperatures, causing agglomeration into nanoparticles.⁶ Hence, low surface concentrations are generally used since it is often energetically favorable to form dimers, trimers, or larger clusters with increasing metal loading. For example, Qiao et al.4 observed exclusively single-atom species

on a 0.17 wt % Pt/FeO_x but Pt rafts and small clusters in their 2.5 wt % Pt/FeO_x sample. To preserve isolated atoms, DeRita et al. used only 1 Pt atom per TiO₂ support particle (0.05 wt % Pt). Two recent reviews pointed out the need to achieve high metal loadings as a significant challenge. 7,8 Recent work on nonoxide supports $^{9-11}$ has demonstrated the ability to

Received: December 6, 2018 Revised: February 5, 2019 Published: February 14, 2019



Department of Chemical and Biological Engineering and Center for Microengineered Materials, University of New Mexico, Albuquerque, New Mexico 87131, United States

[‡]Department of Chemistry and Chemical Biology, University of New Mexico, Albuquerque, New Mexico 87131, United States

[§]Department of Material Science and Engineering, Jingdezhen Ceramic Institute, Jingdezhen 333403, China

Voiland School of Chemical Engineering and Bioengineering, Washington State University, Pullman, Washington 99164, United States

¹Davidson School of Chemical Engineering, Purdue University, West Lafayette, Indiana 47907, United States

[#]Tascon GmbH, Mendelstr. 17, 48149 Münster, Germany

⁷ION-TOF GmbH, Heisenbergstr. 15, 48149 Münster, Germany

⁸JEOL LTD, 3-1-2 Musashino, Akishima, 196-8558 Tokyo Japan

⁹Institute for Integrated Catalysis, Pacific Northwest National Laboratory, Richland, Washington 99354, United States

generate high metal loadings of single atoms, but stabilizing single atoms of platinum group metals on oxide supports remains a challenge.

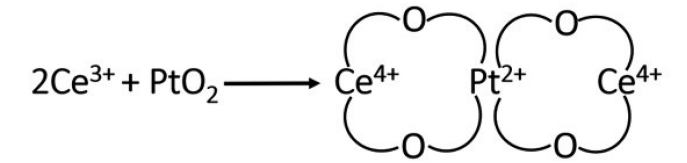
We work on ceria because this support is unique in that atomically dispersed Pt species can be formed simply by treating the catalyst at high temperatures in flowing air. ¹² In our previous work, we physically mixed a Pt/alumina sample with ceria to form atomically dispersed Pt. ¹² However, a similar result was also achieved by depositing the Pt precursor on the support via impregnation. ¹³ This method of synthesis (atom trapping) represents a facile approach to prepare single-atom catalysts. ¹⁴ The focus of this report is on understanding how single-atom catalysts could be prepared using readily available commercial precursors and supports, and exploring the upper limit for depositing stable single atoms of Pt.

When Pt metal is heated to high temperatures in the presence of oxygen, volatile PtO₂ is formed. ¹⁵ Due to the weak interaction with supports such as silica, 16 the PtO₂ condenses forming large particles. The interaction with ceria (111) terraces is also weak, but 4-fold sites on CeO₂(100) pockets were identified by Bruix et al.¹⁷ as strong binding sites for Pt ions. Using a model CeO2 cluster, it was demonstrated via density functional theory (DFT) calculations that the deposited Pt atoms were oxidized to form Pt2+ leading to a corresponding reduction of two Ce^{4+} cations to form Ce^{3+} . In our previous work, 12 we found that polyhedral ceria and nanorods were very effective at binding Pt and stopping sintering, but ceria cubes which expose (100) facets were not very stable when heated at elevated temperatures. 12 The ceria (111) facet is the dominant exposed surface in powder samples; however, this surface does not provide 4-fold sites for binding Pt. Dvorak et al. 18 used STM on model ceria CeO₂(111) surfaces to identify sites where Pt single atoms could be strongly bound. They concluded that step sites could achieve a 4-fold coordination and lead to stable Pt²⁺ species. Here we explore whether similar surface sites can also exist on high-surface-area ceria powders.

By using thermally stable commercial ceria powders, we demonstrate here that high (3 wt %) loading of Pt can be stabilized exclusively in the form of isolated single atoms without forming any clusters or aggregates. Only after exceeding the saturation capacity of this ceria support do we detect metallic Pt particles. The nature of the Pt species was studied using surface-sensitive probes such as Low Energy Ion Scattering (LEIS) and X-ray Photoelectron Spectroscopy (XPS) and the coordination to the support was studied using Extended X-ray Absorption Fine Structure (EXAFS) measurements and Density functional theory (DFT) calculations. Aberration Corrected-Scanning Transmission Electron Microscopy (AC-STEM) provides unambiguous evidence of the exclusive presence of atomically dispersed Pt, and this is also confirmed by Diffuse Reflectance Infrared Fourier Transform Spectroscopy (DRIFTS) and CO oxidation reactivity. These results are supported by DFT calculations. We conclude that the stability of Pt single atoms is a result of a reaction between the mobile PtO₂ and under-coordinated Ce³⁺ sites on the catalyst support as shown in Scheme 1.

The ease of reduction of Ce⁴⁺ to Ce³⁺ and formation of oxygen vacancies in ceria supports is well-known¹⁹ and utilized for automotive exhaust catalysis for oxygen storage.²⁰ However, our method of synthesis involves heating the sample to 800 °C in flowing air, a temperature at which we would expect to see only a low concentration of oxygen vacancies. As

Scheme 1. Mobile Pt Species Provide the Oxygen Needed To Bind to Under-Coordinated Ce³⁺ Sites at Step Edges^a



^aSharing of oxygen atoms derived from PtO_2 helps to form covalent bonds with single atoms of Pt^{2+} leading to the stability of the single-atom species. The four-fold sites are provided at (111) step edges, which are plentiful on ceria powder samples. The synthesis at elevated temperatures in air ensures that the ceria surface is free of any adsorbates, allowing facile reaction of Pt with the support.

we show here, all polyhedral ceria particles possess surface steps, and these represent sites where we can find undercoordinated Ce³⁺ cations which are capable of reacting with the mobile PtO₂ species. In Scheme 1, the Pt brings with it the oxygen atoms that are shared with the Ce³⁺ transforming it to Ce⁴⁺ while forming a covalent bond with the support. The method of synthesis is fundamentally different from conventional aqueous impregnation, ²¹ where a sheath of hydroxyls prevent the formation of direct bonds to the support. Scheme 1 helps explain the strong binding of Pt to the support, which is essential for the formation of thermally stable single atoms.

The results presented here shed light on an important attribute of ceria supports: the ability to slow the sintering of Pt. The sinter-resistance of ceria supports has been previously explained in terms of its ability to lower the free energy of metal nanoparticles²² and thereby lowering the driving force for sintering. Here we show that it is the trapping of mobile Pt species that might also be important for understanding why ceria is so effective at preventing catalyst sintering. Catalyst regeneration and burning of coke deposits always involves high-temperature calcination. Hence, the insights gained from understanding surface sites that help to trap mobile Pt species on an industrial catalyst support will be of broad interest to the field of heterogeneous catalysis.

2. METHODS

2.1. Experimental Details. We used tetraamine platinum nitrate $(Pt(NH_3)_4(NO_3)_2)$ obtained from Sigma-Aldrich as the Pt precursor, and it was deposited on high-surface-area ceria powder (obtained from Solvay, grade HSA 5) using incipient wetness impregnation. We prepared samples containing 1, 2, 3, and 4 wt % of Pt/ceria. The pore volume of ceria (0.6 mL/g) was determined by first wetting the dry ceria powder with water. Impregnation of the platinum precursor was done to fill the pores of ceria. The tetraamine platinum nitrate solution was loaded on ceria in multiple aliquots and dried at $110\ ^{\circ}\text{C}$ for 4 h until all the water evaporated in air after each impregnation. The samples were then calcined in a tube furnace with $100\ \text{mL/min}$ of air for $10\ \text{h}$ in air at $800\ ^{\circ}\text{C}$. The furnace temperature was ramped up at $1\ ^{\circ}\text{C}$ per minute.

The Pt loading was determined by Inductive Coupled Plasma-Optical Emission Spectroscopy (ICP-OES), via electron probe microanalysis as well as Transmission Electron Microscopy-Energy Dispersive Spectroscopy (TEM-EDS). For the TEM analysis, a small amount of the powder sample was put in an agate mortar and ground with ethanol to create a suspension. A drop of this suspension was deposited on a 3

mm holey carbon grid. Transmission electron microscopy (TEM) was performed using a JEOL 2010F microscope operated at 200 kV with a Schottky emitter. The analysis was performed on 10 regions of the sample, the average composition was reported. Some of the samples were also analyzed via Scanning Electron Microscopy (SEM) using a Hitachi S-5200 operated at 2 kV. For Energy Dispersive Spectroscopic (EDS) analysis, we used an Oxford Aztec system, with the microscope operated at 10 kV. AC-STEM images were obtained using a JEOL NeoARM equipped with a cold field emitter and the UHR polepiece (resolution 0.071 nm). X-ray Diffraction (XRD) was performed using the Rigaku Smartlab instrument operated at 40 kV and 40 mA equipped with a D/teX 1-D detector and a sealed tube Cu target X-ray source. Data was collected at 6 degrees/min with a 0.02-degree step. The XRD patterns were analyzed using whole pattern, Rietveld analysis, using the MDI Jade software package. Brunauer, Emmett, and Teller (BET) surface area measurements were performed on a Micromeritics Gemini 2360 multipoint analyzer using N₂ adsorption at −196 °C.

CO oxidation was chosen as a probe reaction. The reaction rate measurements were performed using 1/4 in. diameter Utube with 20 mg of sample. The gas flow rates for CO oxidation were the following: CO 1.5 mL/min, O₂ 1 mL/min, and He 75 mL/min and temperature ramp rate was at 2 °C/ min. The as-prepared, air-exposed catalyst was loaded into the reactor (or the DRIFTS cell) and temperature was increased to 300 °C under He. Once at 300 °C, a pretreatment with 10% O2 was performed for 30 min. The gas was switched to He, the catalyst cooled to the reaction temperature, and CO oxidation measurements were performed. The total pressure during CO oxidation was 83.3 kPa, the atmospheric pressure in Albuquerque. The products were analyzed by an Agilent Micro GC. For obtaining Arrhenius plots, the measurements were performed isothermally at low conversions, using a similar reaction set up. In separate experiments, the catalyst surface during CO oxidation reaction was monitored using DRIFTS and Mass Spectrometry (MS). The infrared spectrometer used was a Tensor 27 from Bruker, coupled with a Praying Mantis Diffuse Reflection Accessory from Harrick. The MS used was a ThermoStar GSD 320 T Quadropole Mass Spectrometer (QMS) from Pfeiffer Vacuum, using a Secondary Electron Multiplier (SEM). DRIFTS was performed using a Harrick cell which allowed treatment of

LEIS was used to quantify the concentration of Pt atoms on the surface. This technique²³ selectively detects the topmost atoms, unlike XPS which probes deeper into a sample. The experiments were carried out using an IONTOF Qtac 100 instrument which is a dedicated LEIS instrument equipped with a double toroidal analyzer for the energy analysis of the backscattered ions. The analyzer has a large solid angle of acceptance (full 360° azimuth), while the scattering angle is fixed at 145°. This gives, in combination with parallel energy detection, a high sensitivity while maintaining the mass resolution. We used He⁺ as well as Ne⁺ with ion energy 3 and 5 keV and current 5 and 2 nA, respectively, to analyze the surface concentration of Pt²⁺ ions in the Pt/CeO₂ catalysts. The area scanned per sample by these two ions was $2 \times 2 \text{ mm}^2$ and the ion flux given to the samples was 1.4×10^{14} ions/cm² and 2.8×10^{13} ions/cm² respectively. The spectra for the Pt reference were analyzed within a $1.5 \times 1.5 \text{ mm}^2$ sputter crater over an area of 1×1 mm². The analysis time was adjusted such

that the surface damage was the same as for the other spectra. Assuming a sputter coefficient of 0.1 for He and 1 for Ne, this will lead to a surface damage of 1% and 2% at the end of the analysis. XPS was performed using a Kratos Axis Ultra photoelectron spectrometer equipped with a monochromatic Al K α source operating at 300 W. The base pressure was 2.7×10^{-8} Pa, and operating pressure was 2.7×10^{-7} Pa. XPS was performed in order to study the chemical state of the Pt catalyst. Analysis of the XPS spectra was performed using CasaXPS software.

X-ray absorption spectroscopy (XAS) was performed at the 10 ID beamline at the Advanced Photon Source (APS) at Argonne National Laboratory. Air exposed samples, asprepared after 800 °C calcination were used for the analysis. Samples for XAS analysis were ground into a fine powder and mixed with a 50/50 mixture of boron nitride/PVPP. The mixture was then pressed into a 7 mm pellet for analysis. Samples were measured in fluorescence mode using a Lytle detector with Soller slits and a Zn foil filter. A platinum foil was measured concurrently in transmission mode as an energy reference. Data analysis was performed using WinXAS 3.1 software.²⁴ Phase and amplitude functions for the fitting of Pt EXAFS data were extracted from experimental references. Pt-Pt scattering phase and amplitude was extracted from platinum foil (12 neighbors, 2.77 Å). Pt-O scattering phase and amplitude was extracted from Na₂Pt(OH)₆ (6 neighbors, 2.05 Å). Fourier transforms were taken over a k range of 3-12.5Å⁻¹. Fits in R space for oxide only samples were done over a range of 1.0-2.0 Å. For samples with metallic scattering, the fit range was over 1.0-3.2 Å. Fits were performed on isolated first shell scattering in R space. R space fitting was accomplished by fixing the Debye-Waller factor and allowing the bond distance, coordination number, and E0 to vary. After a satisfactory fit was obtained, the Debye-Waller factor was adjusted while allowing the coordination number to vary to obtain a best fit on isolated first shell scattering k space data.

2.2. Computational Details. All spin-polarized DFT calculations were carried out with the Vienna Ab initio Simulation Package (VASP)^{25,26} with the PW91 functional.²⁷ The electronic wave functions were expanded in plane waves up to a cutoff energy of 400 eV and the ionic core electrons were approximated by the projector augmented-wave (PAW) method.²⁸ To describe properly the behavior of electrons in f orbitals of Ce in CeO₂, the DFT + U method with U = 4.5 eV was used.²⁹

For studying oxidized Pt clusters, an O-terminated slab of $CeO_2(111)$ with a six atomic layer unit cell of a=13.33 Å and b=15.39 Å including 32 Ce and 64 O atoms was employed. For studying the migration of the PtO_2 species on $CeO_2(111)$, a smaller six atomic-layer unit cell of 7.65×13.25 Ų with 16 Ce and 32 O atoms was adopted. The calculated CeO_2 lattice parameter of 5.44 Å was consistent with the previously reported experimental and theoretical values. In our calculations, the top three atomic layers and the adsorbates were allowed to relax while the bottom three atomic layers were fixed. Both $1 \times 1 \times 1$ and $2 \times 1 \times 1$ k-point meshes were adopted to sample the Brillouin zone for the model of oxidized Pt clusters and PtO_2 species on $CeO_2(111)$, respectively, which was tested to be converged.

The step-edge model used in this wok was similar to those reported in previous theoretical studies of Pt interaction with CeO₂ surfaces, specifically the Step-II and Step-U Models used in ref 18 and ref 32, respectively. A step was constructed by

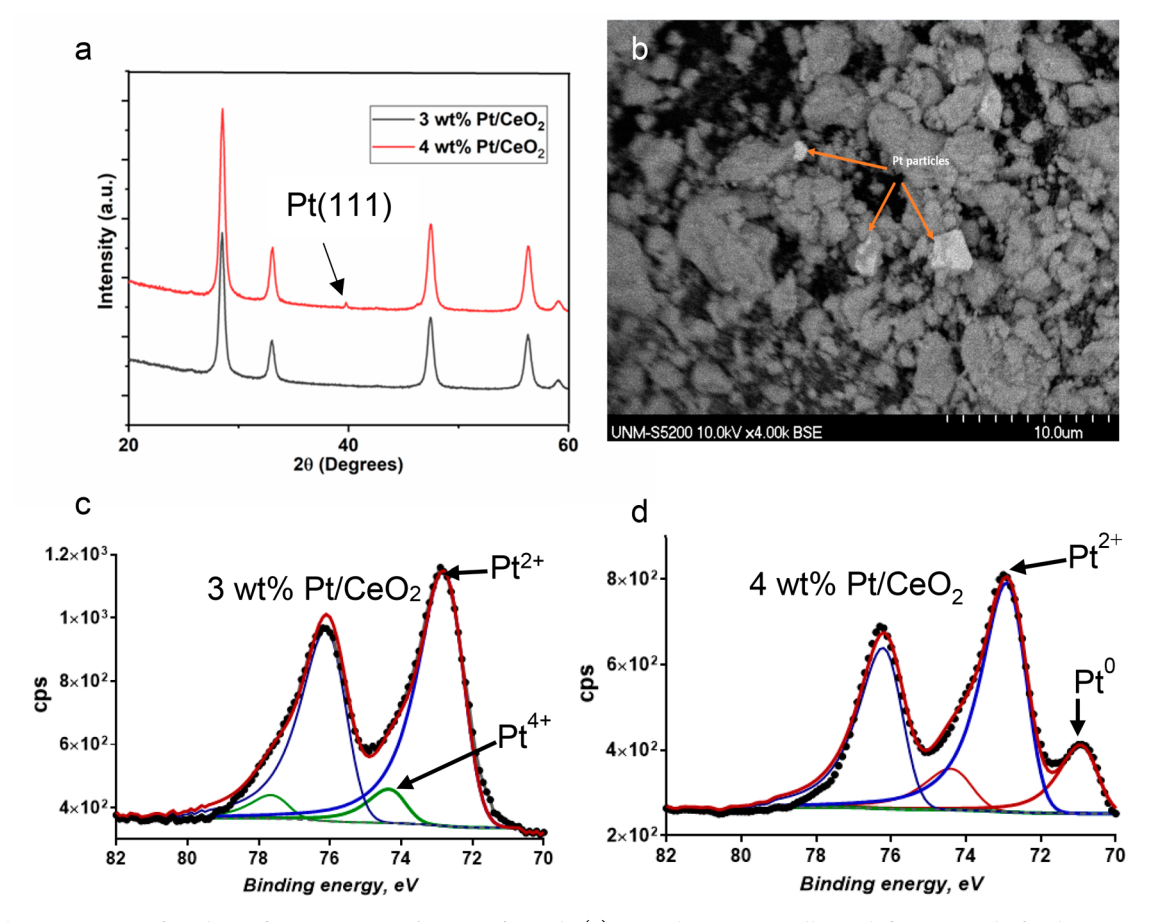


Figure 1. Characterization of catalysts after aging at 800 $^{\circ}$ C in air for 10 h. (a) XRD shows no metallic Pt diffraction peaks for the 3 wt $^{\circ}$ Pt sample but a well-defined metallic Pt(111) peak in the 4 wt $^{\circ}$ sample. (b) SEM image showing the presence of large Pt particles in the 4 wt $^{\circ}$ Pt/CeO₂. (c) XPS analysis of the 3 wt $^{\circ}$ sample showing that the Pt is primarily in the +2 oxidation state. (d) 4 wt $^{\circ}$ Pt sample shows the presence of metallic Pt coexisting with the ionic Pt.

adding three additional atomic layers (2 O layers and 1 Ce layer) on the $7.65 \times 13.25 \ \text{Å}^2 \ \text{CeO}_2(111)$ slab with six atomic layers. Thus, the model step consists of nine atomic Ce/O layers with 20 Ce and 40 O atoms. During the structural optimization, the atomic positions of the lowest three CeO₂ atomic layers were constrained while the other layers as well as the adsorbates were fully relaxed. The k-point mesh was set to be $2 \times 1 \times 1$. A vacuum space of 14 Å or larger was employed between the neighboring interleaved slabs for all the surface models.

The adsorption energy of a pertinent species was computed as follows: $E_{\rm ads} = E_{\rm (adsorbate+surface)} - E_{\rm (free\ molecule)} - E_{\rm (free\ surface)}$. A transition state (TS) between an initial state (IS) and final state (FS) was determined using the climbing image nudged elastic band (CI-NEB) method. The total energy difference was less than 10^{-4} eV, and the convergence of relaxation was checked with the 0.05 eV/Å criterion.

3. RESULTS AND DISCUSSION

3.1. Upper Limit for Loading Atomically Dispersed Pt.

To explore the upper limit for loading single atoms of Pt on ceria, we prepared catalysts ranging from 1–4 wt % Pt using a thermally stable high surface area commercial ceria (Solvay grade HSA 5). After deposition of Pt, the samples were treated in flowing air at 800 °C for 10 h. As shown in Figure 1a, no Pt peak is seen via X-ray diffraction (XRD) on the 3 wt % sample indicating that the Pt is atomically dispersed, but the 4 wt % Pt

sample shows a well-defined Pt(111) reflection at 39.7°. The presence of large Pt particles is also confirmed via SEM, Figure 1b, indicating that the saturation coverage of atomically dispersed Pt has been exceeded in the 4 wt % Pt/ceria sample. The formation of metallic Pt during 800 °C treatment in air may seem surprising. It is known that volatile PtO2 is formed when Pt is heated in air, 15 but as we show later in section 3.3, this PtO2 does not nucleate on ceria because small clusters of Pt oxide are not stable at this temperature. Instead, large Pt particles are formed when Pt catalysts are aged in air³³ because the PtO2 can adsorb on the step edges of metallic Pt ⁴ As shown in this work, ceria has the remarkable particles.3 ability to trap this volatile Pt at atomic dispersion at concentrations up to 3 wt %, preventing the formation of metallic Pt particles.

The as-prepared samples were analyzed via X-ray photoelectron spectroscopy (XPS) to determine the concentration of Pt and its oxidation state. The quantification of the peaks and details of the Ce 3d and Pt 4f regions is presented in the Supporting Information (SI, Figure S1–S2 and Table S1). XPS analysis of the 3 wt % Pt sample (Figure 1c) shows that the Pt is present in an oxidized form primarily in the Pt²⁺ oxidation state (72.5 eV) with a very small contribution from Pt⁴⁺ (74.5 eV). The relative contribution from the Pt⁴⁺ peak decreases from 12.2% in the 1 wt % sample to 5.1% in the 3 wt % sample (Figure S1 and Table S1). The 4 wt % Pt sample is very different (Figure 1d, S2, and Table S3) and shows a prominent

metallic Pt peak at 70.6 eV. A linear relationship between the XPS determined Pt/Ce ratio, and the bulk Pt loading is indicative of atomic dispersion of the Pt since the ceria particle size and the BET surface areas of these samples are very similar. Above the saturation capacity of ceria (4 wt % Pt), we see a bimodal distribution: Pt single atoms (as inferred from XPS, Figure 1c,d) coexisting with Pt particles that are typically ~100 nm or larger. No small Pt clusters are visible in the HAADF-STEM image (Figure S3) and via TEM (Figure S4).

3.2. Nature of Atomically Dispersed Pt. The nature of the Pt species on ceria was determined via electron microscopy. In the 4 wt % Pt/CeO2 sample, the large Pt particles (usually ~100 nm or larger) can be seen via SEM (Figure 1b) and their presence is evident in the XRD and XPS data (Figure. 1a,d). The presence of atomically dispersed Pt is evident from the Pt2+ peak via XPS, but it is difficult to image with a conventional TEM/STEM (JEOL 2010F) in HAADF images which are shown in Figure S3. When regions that do not contain large particles are analyzed via EDS (Figure S4), the amount of atomically dispersed Pt can also be quantified. The concentration of crystalline Pt (large particles) can be quantified via XRD, as shown in Figure S5. The hightemperature synthesis of these samples (800 °C in air) yields atomically dispersed Pt and only at high metal loadings do we see large Pt particles coexisting with atomically dispersed Pt. There are no other species in the sample. Hence, by performing TEM-EDS analysis of regions of the sample that do not contain any detectable metallic Pt particles (as shown in Figure S3 and S4), we obtain a direct measure of atomically dispersed Pt. The sum of Pt detected via quantitative Rietveld refinement of XRD data (Figure S5) and atomically dispersed Pt via TEM-EDS, adds up to the total Pt content, allowing us to complete the mass balance for Pt, as shown later in Table 1. Direct evidence for the presence of Pt single atoms is obtained via aberration corrected scanning transmission electron microscopy (AC-STEM) using the JEOL NeoARM microscope.

The AC-STEM images of the 3 wt % Pt/ceria in Figure 2a-d are replete with white dots, most of which come from Ce atom columns. When the Ce atoms are lined up along the viewing direction (see particle A in Figure 2a), strong channeling contrast from Ce cations makes it very difficult to

Table 1. Surface Concentration of Pt Determined by TEM-EDS, LEIS, and XPS

	BET surface area (m²/g)	ICP- OES analysis	atoms of Pt/nm² calculated	atoms/nm² from LEIS	Pt/Ce ratio from XPS
blank CeO ₂	130	-	-	-	-
1 wt % Pt/CeO ₂	90	0.932	0.32	0.37	0.022
2 wt % Pt/CeO ₂	90	1.71	0.59	0.54	0.037
3 wt % Pt/CeO_2	95	3.06	0.99	0.77	0.063
4 wt % Pt/CeO ₂	101	4	1.01 ^a	0.85	0.066

^aThe 4 wt % Pt/ceria sample contains 0.8 wt % of metallic Pt and 3.2 wt % of atomically dispersed Pt, the latter value was used to calculate the surface concentration of single atoms of Pt.

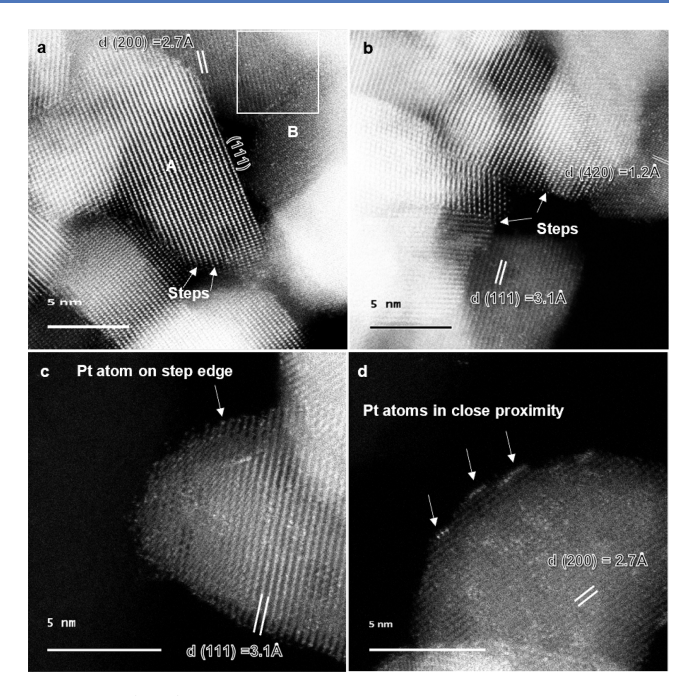


Figure 2. (a–d) AC-STEM images of 3 wt % Pt/ceria. Particle A oriented along [112] with strong contrast from the Ce atom columns, while particle B is oriented off the zone axis making it easier to detect the Pt single atoms. Pt atoms appear bright compared to the contrast of the support. Surface steps are a common feature and Pt can be seen to decorate the step edge in (c) and Pt atoms are found in close proximity in (d).

discern the isolated Pt atoms. Particle B in Figure 2a is oriented off the zone axis with faint lattice contrast from the ceria support. The bright dots that stand out against the background of the ceria support indicate the presence of isolated Pt atoms. The boxed region in Figure 2a shows bright dots corresponding to the Pt atoms lined up with the underlying ceria (200) lattice planes. In this boxed region, we counted 25 atoms (see Figure S6) in an area of 25 nm², which indicates a surface concentration of 1 atom Pt/nm² that is in excellent agreement with estimates from bulk elemental analysis and BET surface area measurement and LEIS as shown later in this manuscript. The AC-STEM images also show that these polyhedral ceria particles expose (111) facets with surface steps, indicated by arrows on Figure 2a-c. Figure 2d shows that at high metal loading, the Pt atoms can exist in close proximity. Overlap between such closely spaced atoms in the viewing direction could cause shadowing and explain the lower apparent surface coverage by LEIS for the higher loading samples when compared with other techniques.

The surface concentration of Pt was independently measured using low energy ion scattering (LEIS), a technique that can selectively analyze surface atoms of the sample. In this method, ²³ the sample is exposed to ions of known kinetic energy. The backscattered ions result from elastic collisions with the topmost atoms in the surface. The energy of the backscattered ions, which is dependent on the mass of the scattering partner, enables the identification of the surface atoms. In this work, 3 keV ⁴He⁺ ions and 5 keV ²⁰Ne⁺ ions were used (Figure S7). With ⁴He⁺ ions there was overlap between the Pt and Ce signals, but with the heavier ²⁰Ne⁺ ions, the peaks of Ce and Pt were well resolved to allow quantification of the surface signal (Figure 3a). The method of calculation is described in the SI (Tables S4 and S5).

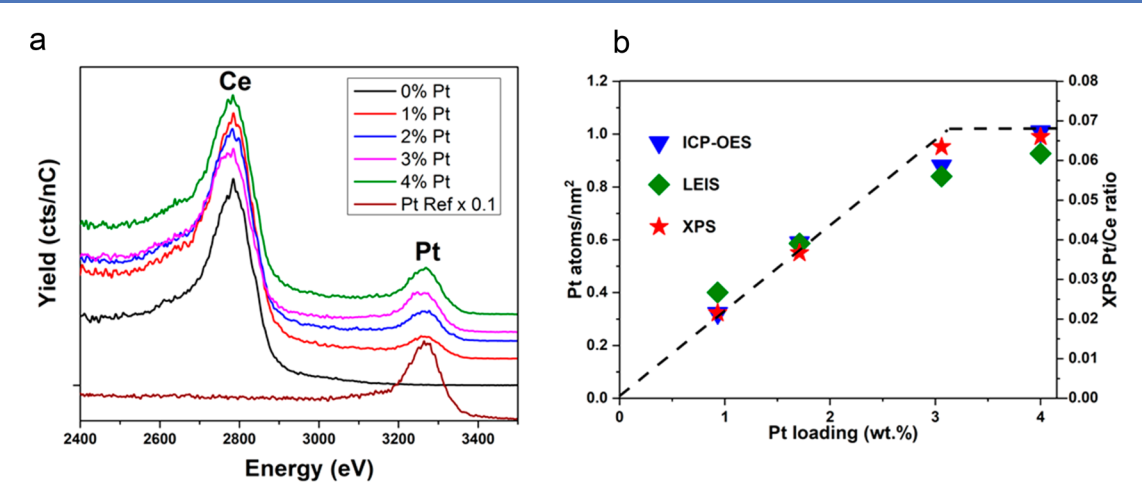


Figure 3. (a) 5 keV ²⁰Ne⁺ LEIS spectra for the samples after O atom treatment, compared to a sputter cleaned Pt foil (scaled 0.1×). (b) A plot showing surface concentration of Pt derived from bulk elemental analysis and LEIS (left axis) and XPS Pt/Ce ratio (right axis) as a function of metal loading. At 4 wt % Pt, the sample shows coexistence of metallic Pt and atomically dispersed Pt.

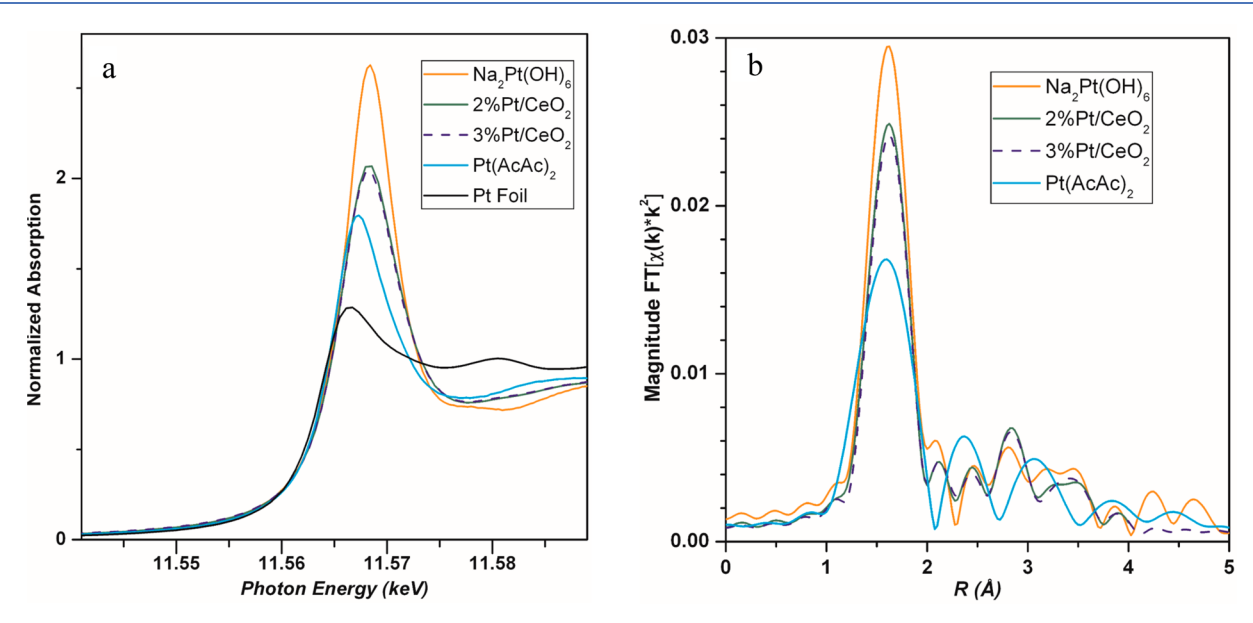


Figure 4. (a) Pt L3 XANES from 11.54–11.59 keV of Na₂Pt(OH)₆, Pt(AcAc)₂, Pt foil, 2 wt % Pt/ceria, and 3 wt % Pt/ceria after heating in air at 800 °C. (b) Fourier transform magnitude of the EXAFS.

Since samples containing 1-3 wt % Pt only show single-atom Pt species and no metallic Pt, we can calculate the surface concentration of atomically dispersed Pt from the measured BET surface areas and the bulk elemental analysis (Table 1). The ceria as-received has a surface area of $130~\text{m}^2/\text{g}$, but after heating the ceria at 800~°C for 10~h, its surface area drops to $60~\text{m}^2/\text{g}$. Loading the Pt on ceria and aging at 800~°C for 10~h under flowing air helps to maintain high surface area. This synergistic effect of trapped Pt on preserving the surface area of ceria was also mentioned in our previous work. 12

For the 4 wt % Pt sample, because of the coexistence of metallic Pt and single-atom species, we analyzed regions devoid of metallic Pt particles via TEM-EDS and determined the saturation loading of single-atom Pt species to be ~3.2 wt % (Figure S4). The amount of Pt giving rise to the XRD peaks was also quantified by whole pattern fitting (Figure S5 and Table S2), allowing us to complete the mass balance for the Pt species. This combination of XRD and TEM-EDS analysis

allows determination of the upper limit for atomically dispersed Pt in this sample to be ~ 1 atom/nm² (Table 1).

The agreement between the surface concentrations calculated via bulk elemental analysis and BET surface area and LEIS is remarkably good (Table 1), especially since LEIS provides a direct measure of surface concentration without any normalization. The surface sensitive detection of Pt in these samples via ion scattering confirms that it is located on the surface, and not buried, or doped into the ceria. For the 3 wt % and especially 4 wt % samples, there is a small, but clear, signal reduction (23 and 30% respectively) of the surface Pt detected via LEIS compared with the value determined by bulk elemental analysis and via XPS suggesting the beginning of clustering or some shadowing of the Pt by the support. This is consistent with the electron microscopy results (Figure. 2d), which indicate that Pt atoms are in close proximity at such high metal loadings.

The nature of the Pt species was studied via XAS, which provides information on the oxidation state of Pt and the bond

Tuble 2. Illiuny 515 of Library 5 data on 1 t/ CCC	Table 2. Anal	ysis of	EXAFS	data	on	Pt/	'CeO,
--	---------------	---------	-------	------	----	-----	-------

samples	XANES edge energy (keV)	scattering pair	CN	R (Å)	$\Delta\sigma^2 \ ({ m \AA}^2)$	E_0 (eV)	comment
Pt Foil	11.5640	Pt-Pt	12	2.77	0.0	-0.2	Pt^0
$Na_2Pt(OH)_6$	11.5666	Pt-O	6	2.05	0.0	-0.3	$O_h Pt^{4+}$
$Pt(AcAc)_2$	11.5652	Pt-O	4	2.03	0.0	-0.3	$D_{ m h}$ Pt $^{2+}$
2 wt % Pt/CeO ₂	11.5657	Pt-O	4.8	2.04	0.0	-0.2	Pt ²⁺ single site
3 wt % Pt/CeO ₂	11.5656	Pt-O	4.8	2.04	0.0	-0.1	Pt ²⁺ single site

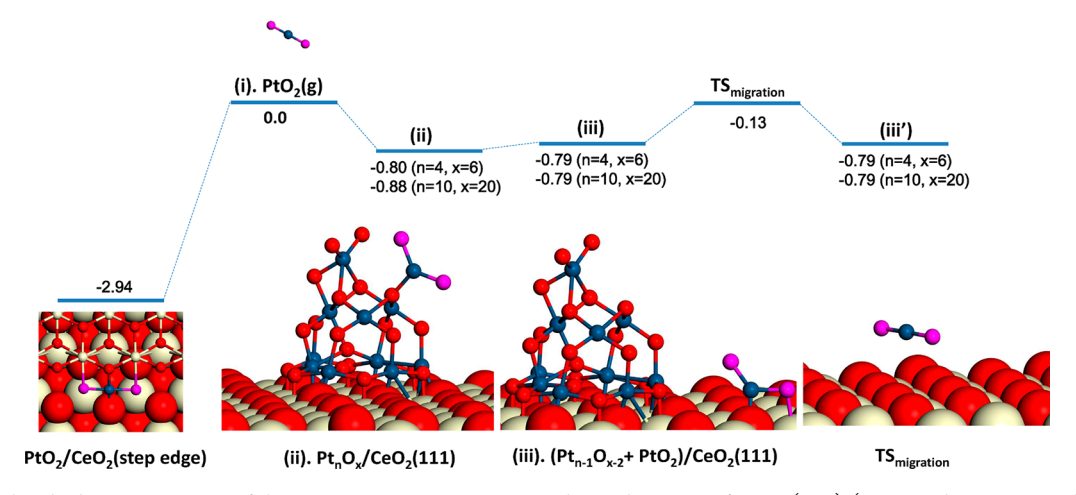


Figure 5. Calculated adsorption energy of the PtO₂ species on CeO₂ step edge and on Pt_nO_x/CeO₂ (111) (n = 4 and 10, x = 6 and 20) as well as the energy cost for the detachment of this PtO₂ species onto the CeO₂(111) surface. The energy barrier for PtO₂ migration on the CeO₂(111) surface is also shown. The corresponding optimized structures along the pathways are also provided. Color: Ce, yellow; lattice O, red; O in PtO₂, purple; Pt, blue.

distances to the neighboring atoms. Figure 4a shows the X-ray absorption near edge structure (XANES) spectra of several Pt reference compounds and the Pt/ceria samples in the asprepared, air-exposed state. The XANES edge energy of the 2 and 3 wt % Pt sample matches that of Pt(II) acetylacetonate (Table 2). The white line intensity (Figure 4a) of Pt/ceria is slightly higher than Pt(II) acetylacetonate, but not as large as Na₂Pt(OH)₆. XPS results indicate that platinum is present in the +2 state, which rules out changes in the XANES due to oxidation state. Thus, the higher inflection point energy and white line intensity can be attributed to platinum in the catalyst having more oxygen neighbors than Pt(AcAc)₂. The magnitude of the Fourier transform of these catalysts is exactly 16% smaller than O_h Pt(IV) and 25% larger than square planar Pt(II). In these air-exposed samples, the Pt(II) species could be interacting with an additional oxygen to form the fifth Pt-O bond. XPS results demonstrating that Pt⁴⁺ is a minority species also rule out the possibility of a 50/50 mixture of fourcoordinate Pt2+ and six-coordinate Pt4+ which would appear as five-coordinate. The lack of intense second shell Pt-O-Pt scattering typical of platinum oxide clusters confirms that the platinum is present as isolated single atoms. The Pt-O distance (2.04 Å) is also not consistent with Pt doped in the CeO₂ lattice and occupying Ce cation sites which would have 8 O neighbors at 2.34 Å.35

3.3. Exclusive Formation of Atomically Dispersed Pt. The results presented so far indicate that the catalyst asprepared contains exclusively single-atom Pt species which are bound very strongly to the ceria, such that even after exceeding the saturation coverage, we see the coexistence of large Pt particles and single-atom Pt species, but no clusters of Pt. To understand the mechanism for the formation of single Pt species, we investigated theoretically the adsorption of single

Pt species, particularly gaseous PtO_2 , which has been identified as a possible mobile species in Ostwald ripening 33,36 to oxidized Pt clusters on $CeO_2(111)$. By microscopic reversibility, the detachment energy of the gas phase species from the clusters is the same as the adsorption energy with a sign change.

In these calculations, we did not explore metallic Pt clusters because metallic Pt will not be stable under the experimental conditions used for atom trapping. Ganzler et al. 36 showed that small Pt particles are readily oxidized at temperatures as low at 350 °C under oxidizing conditions. Instead, we consider the adsorption of gaseous PtO2 onto two oxidized Pt clusters Pt₁₀O₂₀ and Pt₄O₆ on CeO₂(111). Several adsorption configurations have been explored and the lowest adsorption energies are -0.88 and -0.80 eV, respectively. The small adsorption energies for the PtO2 species on platinum oxide clusters suggest facile release of such species into the gas phase at high temperatures, because of their small detachment energies. These results are consistent with the high vapor pressure of platinum oxide solids and confirm that the PtO₂ species are likely to serve as a mobile species in the gas phase, consistent with the other DFT studies. 33,36

To further explore the possibility of the PtO_2 species serving as the mobile species on $CeO_2(111)$, the energy cost for its detachment from the platinum oxide clusters $Pt_{10}O_{20}/CeO_2(111)$ and $Pt_4O_6/CeO_2(111)$ onto the $CeO_2(111)$ surface is calculated. The PtO_2 species adsorbs on $CeO_2(111)$ with Pt on the oxygen top site and one of its oxygens connecting to a lattice Ce (see Figure 5), with a small adsorption energy of -0.67 eV. The small endothermicity of 0.01 and 0.09 eV for this detachment process, respectively, suggests that the formation of adsorbed PtO_2 is possible on $CeO_2(111)$. To understand its migration on the ceria surface,

we have investigated several diffusion pathways of PtO_2 on $CeO_2(111)$. As shown in Figure 5, they have roughly the same diffusion barrier between 0.61 and 0.71 eV, which are quite close to its adsorption energy (-0.67 eV) on $CeO_2(111)$. This suggests the migration is most likely through the gas phase PtO_2 species. Indeed, it can be seen from the transition state structure in Figure 5 that the distance between the PtO_2 species and the surface is about 2.95 Å, with the PtO_2 in collinear geometry, the same as the gaseous counterpart. These results again imply that the gaseous PtO_2 , rather than surface species, is likely to be the main mobile species at high temperatures.

On the other hand, the calculated adsorption energy of PtO₂ at the step site of $CeO_2(111)$ is -2.94 eV, significantly larger than its adsorption energy at the $CeO_2(111)$ terrace (-0.67 eV). The energetics of the detachment and diffusion of PtO₂ species on $CeO_2(111)$ are shown in Figure 5. On the basis of the energetics, it is concluded that the formation of the strongly bound single-atom Pt species (PtO2) at the step site under oxidizing conditions is likely the result of detachment of PtO₂ species from oxidized Pt clusters on ceria terraces into the gas phase, and redeposition of the gaseous PtO2 species onto step sites of ceria. Using DFT, Wang et al.³⁴ concluded that the adsorption of PtO2 on step edges of metallic Pt was only slightly less favorable than the CeO₂(111) step sites. This would explain why large metallic particles are seen only when the saturation concentration of Pt single-atom species is exceeded.

To determine the preferred location of the Pt atoms at step edges, possible structures of Pt on the step sites of $CeO_2(111)$ were considered (Figure 6a-c). The adsorption geometry of a single Pt atom at the CeO_2 step is given in Figure 6a. The Pt is

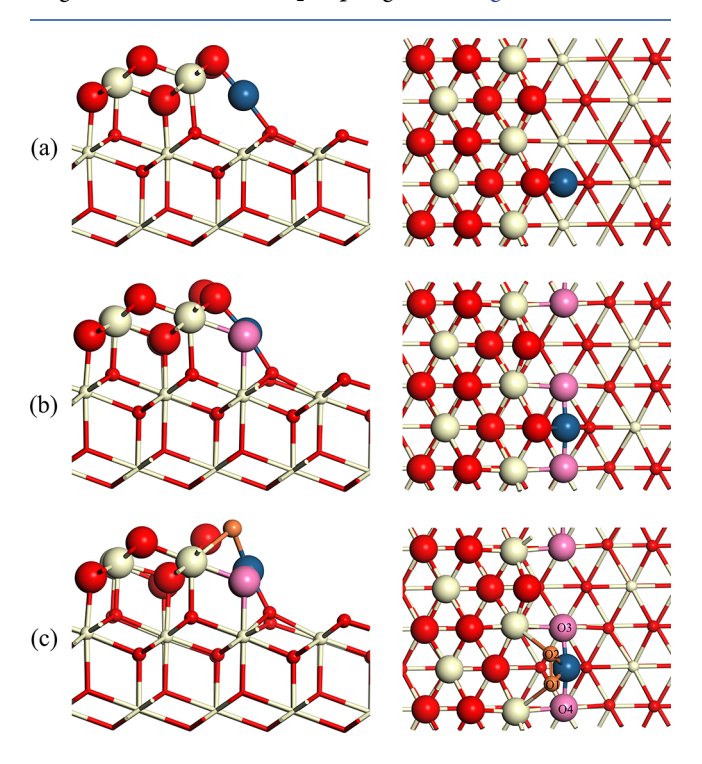


Figure 6. (a) Side and top views of geometry of Pt adsorbed on CeO_2 -step. (b) Pt adsorbed on CeO_2 -step with two excess O atoms. (c) Side and top views of O_2 adsorption on Pt@step-O with a step oxygen vacancy. Color: Ce, yellow; lattice O, red; O in PtO₂, pink; Pt, blue; O in O_2 , orange.

located at a bridge site by binding to two oxygen atoms from the first and second $CeO_2(111)$ layers, with Pt–O bond lengths of 2.00 and 2.00 Å. Its adsorption energy is -4.98 eV, which is in good agreement with the previous value of -5.1 eV.³³ The location of Pt atoms on the ceria steps are consistent with the previously reported STM images of Dvorak et.al.¹⁸

The geometry of a single Pt atom adsorbed on the CeO₂ step site with two excess O atoms is shown in Figure 6b. The two excess oxygen atoms could be due to the PtO2 species from the gas phase, which lands on the step site. The Pt atom is bound to four O atoms, forming a square planar motif with the Pt-O distances of 1.89, 1.89, 1.99, and 2.03 Å. The adsorption energy of Pt is -7.31 eV, indicating the high stability of the structure. The Bader charge of the Pt is 1.13lel, suggesting a Pt2+ character. The Pt4+ species in PtO2 is presumably reduced by the under-coordinated Ce³⁺ at the step edge to Pt2+ (Scheme 1). It is clear that the square-planar geometry (Figure 6b) is more stable than that without the two excess oxygens (Figure 6a). These results are also consistent with the earlier results of Dvorak et al. 18 who noted the beneficial effect of excess oxygen for achieving high concentrations of atomically dispersed Pt. However, in that study the authors found that exceeding the saturation limit caused the appearance of clusters of Pt, which are not seen in our work, which we suspect is due to the different synthesis conditions. In our work, the catalyst is prepared by heating in air at 800 °C, under which condition the smaller clusters of Pt oxide are not stable due to the emission of gaseous PtO2 species.

To understand the five-coordinated species involving Pt, which is suggested by the EXAFS experiment (Table 2), we explored the possibility that one of the Pt-bound O is replaced by O2. This is plausible since the Pt/CeO2 catalyst was prepared in air at high temperatures and the air-exposed samples were analyzed. When an oxygen vacancy is formed at the CeO₂ step site, O₂ can adsorb at the oxygen vacancy. This situation is considered in Figure 6c, where a step O bound to Pt is replaced by O₂ on Pt/CeO₂. The O₂ moiety has both O atoms bonded to Pt and two Ce atoms in the top layer. In this planar configuration, therefore, Pt is bonded with five O atoms with the Pt-O distances of 2.07 Å (Pt-O1), 2.07 Å (Pt-O2), 1.96 Å (Pt-O3), 1.96 Å (Pt-O4) and 2.01 Å (Pt-O5), respectively. This configuration is consistent with the experimental EXAFS averaged bond length of 2.04 Å (see Table 2 and Figure 4). The adsorption energy for O_2 is -1.86eV, which is comparable to the oxygen vacancy formation energy (2.12 eV). The small endothermicity of 0.26 eV makes the substitution of a step O bond to Pt by an O2 molecule quite plausible. When the catalyst is exposed to CO, we expect this adsorbed oxygen to react readily, allowing CO to bind to the Pt²⁺ site on the ceria.

This location of the Pt in both of our DFT models also matches with the AC-STEM images. The Pt atom lies very close to the (111) ceria plane and also on the (200) plane. This explains why our results (Figure 2), and also those of others in the literature, ^{7,8} which show the Pt atoms to be lined up with the ceria lattice planes. These Pt atoms are not actually in substitutional sites, rather they are present on surface steps. Polyhedral ceria particles heated to 800 °C in air show well-defined (111) facets and a multitude of surface steps, some of which are indicated with arrows in Figure 2b and 2c. Since the TEM images are projections of a three-dimensional structure, the Pt atoms on the surface appear as if they lie on specific

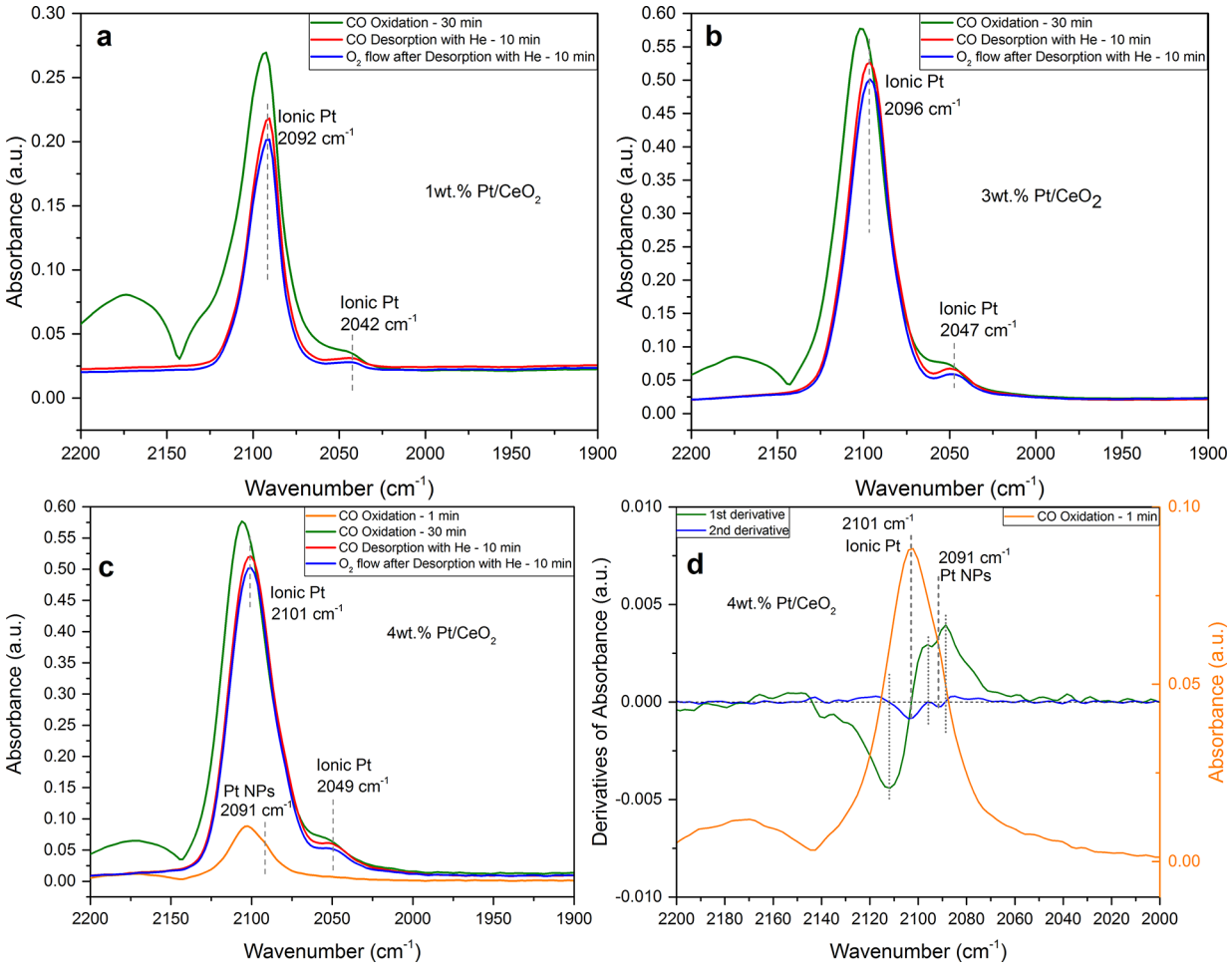


Figure 7. (a) FTIR of adsorbed CO on the 1 wt %Pt/CeO₂ during CO oxidation at 125 °C, and after stopping the CO flow and purging with He, and later while purging with O₂. This shows that the CO is strongly bound to the ionic Pt species. Similar experiment with the (b) 3 wt % Pt/CeO₂ and (c) 4 wt % Pt/CeO₂. The CO adsorption band for the 4 wt % Pt samples suggests an additional component is present, indicated by the 2091 cm⁻¹ band seen most clearly in the spectrum obtained after 1 min of reaction. (d) The 1st and 2nd derivative analysis of the 1 min spectrum shows this feature at 2091 cm⁻¹, which can be assigned to large metallic Pt particles.

ceria lattice planes. Due to the atom mobility induced by the beam, it becomes very difficult to find isolated atoms at the edge of the ceria particles, but they are visible, as seen in Figure 2c

3.4. Reactivity of Atomically Dispersed Pt/CeO₂. To assess the nature of the Pt species under reaction conditions, and their stability, we used DRIFTS while performing CO oxidation at 125 °C. The catalyst was subjected to an oxidative pretreatment to clean off adsorbed impurities, no reduction was performed. Since there was excess oxygen in the feed, the catalyst does not change its state, or get reduced, as evident from the FTIR data. The band of adsorbed CO is similar across the entire range of metal loadings (Figure 7). The position of the band does not change with coverage (Figure 7) consistent with isolated Pt sites. The fwhm (full width at half maximum) of the strongly bound CO is ~ 23 cm⁻¹, considerable broader than the narrow band having a fwhm <10 cm⁻¹ reported by DeRita et al.⁵ These authors used a very low loading of Pt (0.05 wt %) to achieve uniform single-atom sites. The high loading (3 wt %) used in our samples and the different configurations of surface steps on ceria 18 make it likely that there is not one unique configuration for the Pt single sites. The CO adsorption band on the 4 wt % Pt sample (Figure 7c) is further broadened due to a contribution from

metallic Pt present in this sample. This is shown more clearly in the magnified view of the CO band seen initially during CO oxidation on the 4 wt % Pt sample (Figure 7d). The first and second derivative show the presence of a feature at 2091 cm⁻¹ corresponding to metallic Pt. However, the contribution from the metallic Pt sites is not very significant due to the large Pt particles that are present (Figure. 1b) hence the dominant CO species are those on ionic Pt at ~2100 cm⁻¹. This is in contrast to the work of DeRita et al.⁵ where two distinct bands for adsorbed CO were seen already at 0.15 wt % and only the metallic Pt bands were seen at 1 wt % Pt loading. The synthesis conditions used in the present study tend to favor formation of atomically dispersed Pt even at the highest metal loading used (4 wt % Pt) where the excess Pt forms large metal particles.

On these samples, the adsorbed CO on ionic Pt is strongly bound and not easily desorbed in flowing He and neither does it react with O₂ at 125 °C (Figure 7). This is consistent with the low CO oxidation reactivity of these single-atom catalysts at 125 °C as we show next. The frequency of the adsorbed CO band is consistent with the recent DFT investigation of Thang et al.³⁷ where CO on ionic Pt at ~2100 cm⁻¹ would be expected to have strongly bound CO with binding energy larger than 2 eV. The FTIR spectra (Figure 7) of the single-atom catalysts prepared by high temperature vapor phase

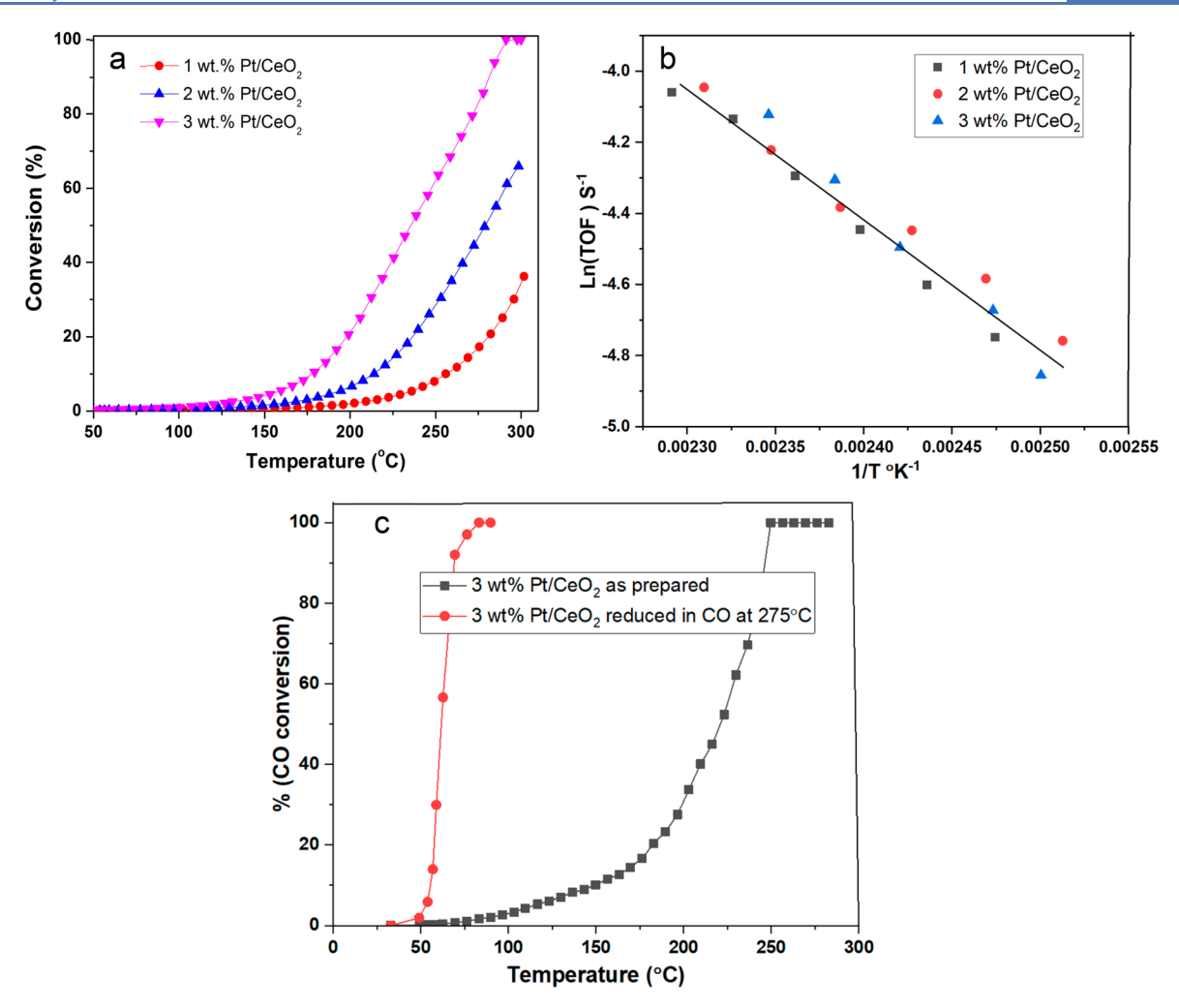


Figure 8. (a) CO oxidation reactivity on the Pt/ceria catalysts, third run reported, demonstrating the stability of the single atoms when using lean conditions (1 sccm of CO, 1.5 sccm of O_2 , 75 sccm of He with 20 mg of catalyst, at a total pressure of 83.3 kPa. (b) Turnover frequency (TOF) as a function of reciprocal temperature. (c) CO oxidation reactivity of the 3 wt % Pt/CeO₂ after reduction in CO at 275 °C.

synthesis on ceria also show a very minor feature in the range of 2042-2049 cm⁻¹. A CO band in this range would normally be associated with metallic Pt, based on the literature. 37,38 However, in our case the catalyst has been prepared by heating at 800 °C in air and then preoxidized prior to performing CO oxidation under lean conditions. Neither AC-STEM nor EXAFS show any metallic Pt particles to be present on this catalyst. Furthermore, this 2042-2049 cm⁻¹ band is not removed when CO flow is stopped and oxygen continues to flow, which is similar to the behavior of the most intense band on our single-atom catalysts (2092-2101 cm⁻¹). On the other hand, CO adsorbed on metallic Pt readily reacts with oxygen when CO flow is stopped. 12 Hence we associate the minor feature seen around 2042-2049 cm⁻¹ to the single-atom Pt species, which represent the only form of Pt seen via AC-STEM and via EXAFS. The catalyst that contains metallic Pt is the 4 wt % Pt/ceria where the Pt particles are large and can be seen via SEM and XRD (Figure 1). This metallic Pt makes only a very modest contribution to CO oxidation activity (see Figure S8). We examined the FTIR results on this catalyst very carefully and found that a small shoulder in Figure 7c might be attributed to metallic Pt. Further derivative analysis of this spectrum suggested that the feature was located at 2089 cm⁻¹. The assignment of this band to metallic Pt is consistent with

CO adsorbed on well-coordinated (i.e., large Pt particles as reported in the literature).³⁸ The CO stretch frequency also happens to be very similar to the intense CO band seen in all of the catalysts reported here (Figure 7a,b). While the assignment of a CO stretches around ~2091 cm⁻¹ to Pt nanoparticles and the 2101 cm⁻¹ feature to ionic Pt (Figure 7c) may be surprising, it is consistent with the literature³⁹ where considerable overlap in the observed CO stretch frequencies on metallic nanoparticles and ionic Pt has been reported. These authors have questioned whether the state of Pt can be unambiguously determined from the CO stretching frequency. Our assignments are based on the physical evidence gathered from a number of characterization techniques. In summary, the similar symmetrical CO band seen with increasing metal loading confirms that ceria provides sites for trapping atomically dispersed Pt at high concentrations (~1 atom/nm 2).

The CO oxidation reactivity measured in a flow reactor is shown in Figure 8. The single-atom state of the catalyst is maintained during reaction as confirmed via FTIR (Figure 7) since there excess oxygen in the feed. These catalysts show increased reactivity with loading, and when expressed as a TOF, the performance is very similar, confirming that the Pt sites over the range of loading (1-3 wt %) is very similar. The

4 wt % Pt/CeO₂ sample contains both metallic Pt as well as atomically dispersed Pt. Since the Pt is present in the form of large particles, adding extra Pt makes only a modest improvement in reactivity (Figure S8). The single-atom catalyst is not the most active form of Pt. The catalyst needs to be activated via high temperature steam treatment, ⁴⁰ or via reduction in CO at 275 °C (Figure 8c). The former treatment creates active hydroxyl groups that enhance the reactivity of the single-atom catalyst. The reduction treatment transforms a portion of the single-atom Pt into nanoparticles, leading to an onset of CO oxidation reactivity at RT and 100% conversion by 80 °C.

The mechanisms for the enhanced reactivity of the reduced Pt catalyst are outside the scope of this work and are presented elsewhere. The single-atom catalyst can therefore be considered the precursor to a very active Pt/ceria CO oxidation catalyst.

4. CONCLUSIONS

The results reported here demonstrate the remarkable behavior of ceria supports that allow trapping of ionic Pt keeping it atomically dispersed. Under-coordinated Ce3+ cations at the ceria step edges can react with PtO2, sharing the oxygens provided by the Pt, to form strong covalent bonds that result in the thermally stable single atoms (Scheme 1). The strong binding of the PtO_2 to step sites on $CeO_2(111)$ and the weak interaction with Pt oxide clusters leads to the exclusive formation of atomically dispersed Pt. Only when the Pt loading is in excess of the saturation capacity that metallic particles of Pt are seen. The results of bulk elemental analysis combined with the BET surface area help identify the upper limit for stabilizing atomically dispersed Pt to be 1 atom/nm², which yields 3 wt % of atomically dispersed Pt on the high surface area ceria support (Solvay HSA 5). The combination of surface sensitive spectroscopic techniques, LEIS, XPS, and DRIFTS, confirms that the Pt atoms are located on the surface of the ceria. The DFT computations show the stable site involves binding of Pt to surface oxygen atoms at the ceria steps with an average distance of 2.04 Å, which is confirmed by EXAFS measurements. The AC-STEM images are consistent with Pt is bound to step edge sites on the ceria.

The results can be considered in the context of catalyst sintering, where growth of metal nanoparticles leads to loss of catalyst activity. 22 The dominant mechanism for catalyst sintering is Ostwald Ripening⁴² wherein mobile single-atom species emitted from the smaller nanoparticles are captured by the larger particles. Calorimetric measurements show that small clusters (and especially single metal atoms) on ceria (111) have higher energy than the bulk metal⁴³ causing them to be less stable and prone to sintering. In contrast, in this work, the transition metal was delivered in the form of a metal oxide, allowing covalent bonds to be formed with the support trapping the single atoms and causing catalyst sintering to be slowed down. The process of atom trapping described here is relevant to industrial catalysts used for hydrocarbon conversions such as dehydrogenation,44 which become poisoned due to carbon deposition and lose activity due to sintering. These industrial catalysts are regenerated via oxidative treatments at ~540 °C to burn the carbon and redisperse the transition metal. Mobile transition-metal oxides such as PtO₂ are formed under these conditions, and their trapping on ceria must be responsible for the sinter-resistance and ease of regeneration of the single atoms from nanoparticles. 13

This work shows that the single atom, ionic Pt, is not active for CO oxidation at low temperatures. However, reduction in CO transforms the single-atom Pt on polyhedral ceria catalyst into a remarkably active low-temperature CO oxidation catalyst. Since the Pt is strongly bound to the support, even after CO reduction a portion of the Pt remains in the form of single atoms. Likewise, in previous work, we found that when the catalyst was prepared via atom trapping, a significant fraction of the Pt remained as single atoms when heated to 680 °C for propane dehydrogenation. In summary, using a high surface area commercial ceria and readily available Pt precursor, we have demonstrated high metal loading of thermally stable Pt single atoms in the form of Pt²⁺ ions, extending single-atom catalysis to the realm of industrial applications.

ASSOCIATED CONTENT

S Supporting Information

The Supporting Information is available free of charge on the ACS Publications website at DOI: 10.1021/acscatal.8b04885.

Additional results of XPS analysis, TEM-EDS, the method for quantifying Pt content via XRD, AC-STEM image confirming surface concentration of Pt, methods used for quantifying LEIS data, reactivity of the entire set of Pt catalysts and the method for calculating TOF (PDF)

AUTHOR INFORMATION

Corresponding Authors

*E-mail: datye@unm.edu. *E-mail: yong.wang@pnnl.gov. *E-mail: slin@fzu.edu.cn.

ORCID ®

Haifeng Xiong: 0000-0002-3964-4677

Xavier Isidro Pereira-Hernández: 0000-0002-7020-0011

Sen Lin: 0000-0002-2288-5415 Hua Guo: 0000-0001-9901-053X Yong Wang: 0000-0002-8460-7410 Abhaya K. Datye: 0000-0002-7126-8659

Notes

The authors declare no competing financial interest.

■ ACKNOWLEDGMENTS

The research was supported by the US Department of Energy (DOE) grant DE-FG02-05ER15712. Additional funding was provided from US National Science Foundation grants EEC-1647722 (CISTAR), the National Natural Science Foundation of China grant 21673040, and the US Air Force Office of Scientific Research grants FA9550-15-1-0305 and FA9550-18-1-0413. XIPH thanks Fulbright Colombia and Colciencias, SZ thanks the China Scholarship Council (201608360178). The research utilized the Advanced Photon Source supported by the U.S. DOE under contract No. DE-AC02-06CH11357 and the Environmental Molecular Sciences Laboratory located at Pacific Northwest National Laboratory, supported by the U.S. DOE Office of Biological and Environmental Research. MRCAT operations and beamline 10-ID are supported by the DOE and the MRCAT member institutions.

REFERENCES

- (1) Yang, X. F.; Wang, A.; Qiao, B.; Li, J.; Liu, J.; Zhang, T. Single-Atom Catalysis: A new Frontier in Heterogeneous Catalysis. *Acc. Chem. Res.* **2013**, *46*, 1740–1748.
- (2) Lin, J.; Wang, A.; Qiao, B.; Liu, X.; Yang, X.; Wang, X.; Liang, J.; Li, J.; Liu, J.; Zhang, T. Remarkable Performance of Ir_1/FeO_X Single-Atom Catalysis in Water Gas Shift Reaction. *J. Am. Chem. Soc.* **2013**, 135, 15314–15317.
- (3) Duarte, R. B.; Krumeich, F.; Van Bokhoven, J. A. Structure, Activity, and Stability of Atomically Dispersed Rh in Methane Steam Reforming. ACS Catal. 2014, 4, 1279–1286.
- (4) Qiao, B.; Wang, A.; Yang, X.; Allard, L. F.; Jiang, Z.; Cui, Y.; Liu, J.; Li, J.; Zhang, T. Single-Atom Catalysis of CO Oxidation Using Pt₁/FeO₂. *Nat. Chem.* **2011**, *3*, 634–641.
- (5) DeRita, L.; Dai, S.; Lopez-Zepeda, K.; Pham, N.; Graham, G. W.; Pan, X.; Christopher, P. Catalytic Architecture for Stable Single Atom Dispersion Enables Site-Specific Spectroscopic and Reactivity Measurements of CO Adsorbed to Pt Atoms, Oxidized Pt Clusters, and Metallic Pt Clusters on TiO₂. *J. Am. Chem. Soc.* **2017**, *139*, 14150–14165.
- (6) Han, C. W.; Iddir, H.; Uzun, A.; Curtiss, L. A.; Browning, N. D.; Gates, B. C.; Ortalan, V. Migration of Single Iridium Atoms and Tri-iridium Clusters on MgO Surfaces: Aberration-Corrected STEM Imaging and Ab Initio Calculations. *J. Phys. Chem. Lett.* **2015**, *6*, 4675–4679.
- (7) Liu, J. Catalysis by Supported Single Metal Atoms. ACS Catal. **2017**, 7, 34–59.
- (8) Liu, L.; Corma, A. Metal Catalysts for Heterogeneous Catalysis: From Single Atoms to Nanoclusters and Nanoparticles. *Chem. Rev.* **2018**, *118*, 4981–5079.
- (9) Li, Z.; Wang, D.; Wu, Y.; Li, Y. Recent Advances in the Precise Control of Isolated Single Site Catalysts by Chemical Methods. *Natl. Sci. Rev.* **2018**, *5*, 673–689.
- (10) Li, H.; Wang, L.; Dai, Y.; Pu, Z.; Lao, Z.; Chen, Y.; Wang, M.; Zheng, X.; Zhu, Y.; Zhang, W.; Si, R.; Ma, C.; Zeng, J. Synergetic Interaction between Neighbouring Platinum Monomers in CO₂ Hydrogenation. *Nat. Nanotechnol.* **2018**, *13*, 411–417.
- (11) Wu, X.; Zhang, H.; Dong, J.; Qiu, M.; Kong, J.; Zhang, Y.; Li, Y.; Xu, G.; Zhang, J.; Ye, J. Surface Step Decoration of Isolated Atom as Electron Pumping: Atomic-Level Insights into Visible-Light Hydrogen Evolution. *Nano Energy* **2018**, *45*, 109–117.
- (12) Jones, J.; Xiong, H.; DeLaRiva, A. T.; Peterson, E. J.; Pham, H.; Challa, S. R.; Qi, G.; Oh, S.; Wiebenga, M. H.; Perreira Hernández, X. I.; Wang, Y.; Datye, A. K. Thermally Stable Single-Atom Platinum-on Ceria Catalysts via Atom Trapping. *Science* **2016**, *353*, 150–154.
- (13) Xiong, H.; Lin, S.; Goetze, J.; Pletcher, P.; Guo, H.; Kovarik, L.; Artyushkova, K.; Weckhuysen, B. M.; Datye, A. K. Thermally Stable and Regenerable Platinum-Tin Clusters for Propane Dehydrogenation Prepared by Atom Trapping on Ceria. *Angew. Chem., Int. Ed.* **2017**, *56*, 8986–8991.
- (14) Datye, A.; Wang, Y. Atom Trapping: a Novel Approch to Generate Thermally Stable and Regenerable Single-Atom Catalysts. *Natl. Sci. Rev.* **2018**, *5*, 630–632.
- (15) Alcock, C. B.; Hooper, G. W. Thermodynamics of the Gaseous Oxides of the Platinum-Group Metals. *Proc. R. Soc. London, Ser. A* **1959**, 254, 551–561.
- (16) Plessow, P. N.; Abild-Pedersen, F. Sintering of Pt Nanopartilces via Volatile PtO_2 Simulation and Comparison with Experiments. *ACS Catal.* **2016**, *6*, 7098–7108.
- (17) Bruix, A.; Lykhach, Y.; Matolínová, I.; Neitzel, A.; Skála, T.; Tsud, N.; Vorokhta, M.; Stetsovych, V.; Ševčíková, K.; Mysliveček, J.; Fiala, R.; Václavu, M.; Prince, K. C.; Bruyère, S.; Potin, V.; Illas, F.; Matolín, V.; Libuda, J.; Neyman, K. M. Maximum Noble-Metal Efficiency in Catalytic Materials: Atomically Dispersed Surface Platinum. Angew. Chem., Int. Ed. 2014, 53, 10525–10530.
- (18) Dvořák, F.; Farnesi Camellone, M.; Tovt, A.; Tran, N.; Negreiros, F. R.; Vorokhta, M.; Skála, T.; Matolínová, I.; Mysliveček, J.; Matolín, V.; Fabris, S. Creating Single-Atom Pt-Ceria Catalysis by Surface Step Decoration. *Nat. Commun.* **2016**, *7*, 1–8.

(19) Paier, J.; Penschke, C.; Sauer, J. Oxygen Defects and Surface Chemistry of Ceria: Quantum Chemical Studies Compared to Experimental. *Chem. Rev.* **2013**, *113*, 3949–3985.

- (20) Mamontov, E.; Egami, T.; Brezny, R.; Koranne, M.; Tyagi, S. Lattice Defects and Oxygen Storage Capacity of Nanocrystalline Ceria and Ceria-Zirconia. *J. Phys. Chem. B* **2000**, *104*, 11110–11116.
- (21) Santhanam, N.; Conforti, T. A.; Spieker, W.; Regalbuto, J. R. Nature of Metal Catalyst Precursors Adsorbed onto Oxide Support. *Catal. Today* **1994**, *21*, 141–156.
- (22) Farmer, J. A.; Campbell, C. T. Ceria Maintains Smaller Metal Catalysis Particles by Strong Metal-Support Bonding. *Science* **2010**, 329, 933–936.
- (23) Brongersma, H. H. Low-Energy Ion Scattering in: Characterization of Materials; Kaufmann, E.N., Ed.; John Wiley & Sons, Inc.: Hoboken, NJ, 2012; pp 2024–2044.
- (24) Ressler, T. WinXAS: a Program for X-ray Absorption Spectroscopy Data Analysis Under MS-Windows. J. Synchrotron Radiat. 1998, 5, 118–122.
- (25) Kresse, G.; Furthmüller, J. Efficient Iterative Schemes for ab initio Total-Energy Calculations using a Plane-Wave Basis Set. *Phys. Rev. B: Condens. Matter Mater. Phys.* **1996**, *54*, 11169–11186.
- (26) Kresse, G.; Furthmüller, J. Efficiency of ab-initio Total Energy Calculations for Metals and Semiconductors using a Plane-Wave Set. *Comput. Mater. Sci.* **1996**, *6*, 15–50.
- (27) Perdew, J. P.; Chevary, J. A.; Vosko, S. H.; Jackson, K. A.; Pederson, M. R.; Singh, D. J.; Fiolhais, C. Atoms, Molecules, Solids, and Surfaces: Applications of the Generalized Gradient Approximation for Exchange and Correlationn. *Phys. Rev. B: Condens. Matter Mater. Phys.* 1992, 46, 6671–6687.
- (28) Blöchl, P. E. Projector Augmented-Wave Method. Phys. Rev. B: Condens. Matter Mater. Phys. 1994, 50, 17953–17979.
- (29) McFarland, E. W.; Metiu, H. Metiu, Catalysis by Doped Oxides. H. Chem. Rev. **2013**, 113, 4391–4427.
- (30) Branda, M. M.; Hernández, N. C.; Sanz, J. F.; Illas, F. Density Functional Theory Study of the Interaction of Cu, Ag, and Au Atoms with the Regular CeO₂(111) Surface. *J. Phys. Chem. C* **2010**, *114*, 1934–1941.
- (31) Gerward, L.; Staun Olsen, J.; Petit, L.; Vaitheeswaran, G.; Kanchana, V.; Svane, A. Bulk Modulus of CeO₂ and PrO₂-An Experimental and Theoretical Study. *J. Alloys Compd.* **2005**, 400, 56–61.
- (32) Liu, J. C.; Wang, Y. G.; Li, J. Toward Rational Design of Oxide-Supported Single-Atom Catalysts: Atomic Dispersion of Gold on Ceria. *J. Am. Chem. Soc.* **2017**, *139*, 6190–6199.
- (33) Graham, G. W.; Jen, H. W.; Ezekoye, O.; Kudla, R. J.; Chun, W.; Pan, X. Q.; McCabe, R. W. Effect of alloy composition on dispersion stability and catalytic activity for NO oxidation over alumina-supported Pt-Pd catalysts. *Catal. Lett.* **2007**, *116*, 1–8.
- (34) Wang, X.; van Bokhoven, J. A.; Palagin, D. Ostwald Ripening versus Single Atom Trapping: Towards Understanding Platinum Particle Sintering. *Phys. Chem. Chem. Phys.* **2017**, *19*, 30513–30519.
- (35) Avakyan, L. A.; Kolpacheva, N. A.; Paramonova, E. V.; Singh, J.; Hartfelder, U.; van Bokhoven, J. A.; Bugaev, L. A. Evolution of the Atomic Structure of ceria-Supported Platinum Nanocatalysts: Formation of Single Layer Platinum Oxide and Pt-O-Ce and Pt-Ce Linkages. J. Phys. Chem. C 2016, 120, 28057–28066.
- (36) Gänzler, A.; Casapu, M.; Maurer, F.; Störmer, H.; Gerthsen, D.; Ferré, G.; Vernoux, P.; Bornmann, B.; Frahm, R.; Murzin, V.; Nachtegaal, M.; Votsmeier, M.; Grunwaldt, J.-D. Tuning the Pt/CeO₂-Interface by In Situ Variation of the Pt Particles Size. *ACS Catal.* **2018**, *8*, 4800–4811.
- (37) Thang, H. V.; Pacchioni, G.; DeRita, L.; Christopher, P. Nature of Stable Single Atom Pt Catalysts dispersed on Anatase TiO₂. *J. Catal.* **2018**, 367, 104–114.
- (38) Kale, M. J.; Christopher, P. Utilizing Quantitative in Situ FTIR Spectroscopy To Identify Well-Coordinated Pt Atoms as the Active Site for CO Oxidation on Al₂O₃-Supported Pt Catalysts. *ACS Catal.* **2016**, *6*, 5599–5609.

(39) Aleksandrov, H. A.; Neyman, K. M.; Hadjiivanov, K. I.; Vayssilov, G. N. Can the State of Platinum Species be Unambiguously Determined by the Stretching Frequency of an Adsorbed CO Probe Molecule? *Phys. Chem. Chem. Phys.* **2016**, *18*, 22108–22121.

- (40) Nie, L.; Mei, D.; Xiong, H.; Peng, B.; Ren, Z.; Hernandez, X. I. P.; DeLaRiva, A.; Wang, M.; Engelhard, M. H.; Kovarik, L.; Datye, A. K.; Wang, Y. Activation of Surface Lattice Oxygen in Single-Atom Pt/CeO₂ for Low-Temperature CO Oxidation. *Science* **2017**, 358, 1419–1423.
- (41) Pereira-Hernandez, X. I.; DelaRiva, A.; Kunwar, D.; Xiong, H.; Sudduth, B.; Engelhard, M.; Kovarik, L.; Murayev, V.; Hensen, E.; Wang, Y.; Datye, A. K. Tuning Pt-CeO₂ interactions by high-temperature vapor-phase synthesis for improved reducibility of lattice oxygen, *Nat. Commun.* **2019**, DOI: 10.1038/s41467-019-09308-5.
- (42) Hansen, T. W.; Delariva, A. T.; Challa, S. R.; Datye, A. K. Sintering of NanoParticles: Particle Migration or Ostwald Ripening? *Acc. Chem. Res.* **2013**, *46*, 1720–1730.
- (43) James, T. E.; Hemmingson, S. L.; Campbell, C. T. Energy of Supported Metal Catalysis: From Single Atoms to Large Metal Nanoparticles. *ACS Catal.* **2015**, *5*, 5673–5678.
- (44) Sattler, J. J. H. B.; Ruiz-Martinez, J.; Santillan-Jimenez, E.; Weckhuysen, B. M. Catalytic Dehydrogenation of Light Alkanes on Metals and metal Oxides. *Chem. Rev.* **2014**, *114*, 10613–10653.